

# Anomalous behavior of control pulses in presence of noise with singular autocorrelation

Daniel Stanek<sup>a</sup>, Benedikt Fauseweh<sup>a,\*</sup>, Christopher Stihl<sup>b</sup>, Stefano Pasini<sup>c,\*</sup>, Götz S. Uhrig<sup>a,\*</sup>

<sup>a</sup>*Lehrstuhl für Theoretische Physik I, TU Dortmund, Otto-Hahn Straße 4, 44221 Dortmund, Germany*

<sup>b</sup>*Institut für Angewandte Materialien - IAM-AWP, Hermann-von-Helmholtz-Platz 1, 76344 Eggenstein-Leopoldshafen*

<sup>c</sup>*Jülich Centre for Neutron Science, JCNS, Forschungszentrum Jülich GmbH, 52425 Jülich, Germany*

## Abstract

We report on the anomalous behavior of control pulses for spins under spin-spin relaxation and subject to classical noise with a singular autocorrelation function. This behavior is not detected for noise with analytic autocorrelation functions. The effect is manifest in the different scaling behavior of the deviation of a real pulse to the ideal, instantaneous one. While a standard pulse displays scaling  $\propto \tau_p^1$ , a first-order refocusing pulse normally shows scaling  $\propto \tau_p^2$ . But in presence of cusps in the noise autocorrelation the scaling  $\propto \tau_p^{3/2}$  occurs. Cusps in the autocorrelation are characteristic for fast fluctuations in the noise with a spectral density of Lorentzian shape. We prove that the anomalous exponent cannot be avoided; it represents a fundamental limit. On the one hand, this redefines the strategies one has to adopt to design refocusing pulses. On the other hand, the anomalous exponent, if found in experiment, provides important information on the noise properties.

## 1. Introduction

The interaction of open quantum systems with an environment, a so-called bath, is the main reason for the decoherence of quantum systems and the loss of well-defined phase relations. Especially in high precision nuclear magnetic resonance (NMR) as well as in quantum information processing (QIP) the decoherence leads to a detrimental loss of signal strength, which is crucial in experimental measurements and in the application of quantum logic gates. Therefore the suppression of decoherence is a long standing issue of great experimental relevance. The two main processes of decoherence are dephasing (spin-spin relaxation, its rate defined by the inverse time  $1/T_2$ ) and longitudinal relaxation (spin-lattice relaxation, its rate defined by the inverse time  $1/T_1$ ). In the present paper we focus on dephasing, i.e., spin-spin relaxation. Thereby, we implicitly assume  $T_1$  to be infinite, i.e., in practice this means  $T_1 \gg T_2$ . But qualitatively, our conclusions pertain also to the case where  $T_1$  and  $T_2$  are of similar magnitude.

One step to overcome dephasing is the application of suitable control pulses to invert the time evolution of the spin or quantum bit. This approach dates back to the spin echo of Erwin Hahn in the fifties [1] which was quickly extended to periodically applied pulses by Carr and Purcell [2] and Meiboom and Gill [3]. Since then a large variety of periodic pulse sequences has been proposed [4–7]. In QIP, this approach is known under dynamic decoupling (DD) [8–10].

Examples of non-periodically repeated cycles of ideal, instantaneous pulses are, e.g., the recursively concatenated sequences (CDD) and the Uhrig dynamic decoupling (UDD) for

the suppression of dephasing. The former require an exponentially growing number of pulses [11] if longer times have to be reached, the latter is much more efficient because it requires only a linearly growing number of pulses [12–16]. UDD pays for power spectra with hard cutoff [14, 15, 17, 18], while for soft cutoffs the Carr-Purcell-Meiboom-Gill sequence works best [19]. Experimental verification of these theoretical proposals are available [20–22]. Furthermore, UDD and other non-periodic sequences have been used to enhance the contrast in magnetic resonance imaging [23, 24].

Experimentally pulses always have a finite duration  $\tau_p$  and they are susceptible to the perturbing influence of the bath. This influence can be reduced by using composite pulses [25–29], by shaping the pulse [30–33], or by applying dynamically corrected gates [34–36]. Of course, shaping of pulses has also been a long-standing issue in NMR. The main aim was to generate *robust* pulses which are only weakly sensitive to pulse imperfections. We can only mention a small part of the abundant literature on this issue [25–29, 37–47], for a book see Ref. [7].

In most experiments of NMR the dominating fluctuations destroying coherence are of *classical* nature, see, e.g., Ref. [48]. Generically the decohering fluctuations are induced by a large number of microscopic and even macroscopic degrees of freedom. At least a part of these degrees of freedom are thermalized at rather high temperatures relative to their generic energy scales. For instance, the nuclear spins can be considered to be in a completely disordered state corresponding to infinite temperature. Thus the resulting fluctuations are thermal fluctuations and their quantum character plays only a minor role [49, 50] so that it can be neglected.

One may think that a strongly disordered state of the decohering bath poses a problem to the preservation of coherence in the systems under study. But the opposite is true: The lack of quantumness of the fluctuations allows us to consider classical

\*Corresponding authors

Email addresses: benedikt.fauseweh@tu-dortmund.de (Benedikt Fauseweh), s.pasini@fz-juelich.de (Stefano Pasini), goetz.uhrig@tu-dortmund.de (Götz S. Uhrig)

fluctuations. This represents a simplification because the classical variables always commute. Hence, the necessary pulse shapes are simpler and the required amplitudes are lower than in the full quantum case. Moreover, the simulation of the decoherence is computationally much simpler.

In this article we present simulations of pulses, which are optimized with respect to their robustness against dephasing from classical baths or from quantum baths. We simulate a single spin coupled to a classical dephasing bath causing spin-spin relaxation and investigate how the autocorrelation  $g(t)$  of the bath affects the performance of the pulses. Our primary finding is that the possibility to optimize the pulse shape depends qualitatively on the autocorrelation function of the noise. For analytic autocorrelation functions, e.g., a Gaussian function  $\log g(t) \propto -t^2$ , the performance of the pulses depends on its shape.

Theoretically, this is expressed by the scaling property of the deviation of the real pulse from the ideal one with respect to the duration  $\tau_p$  of the pulse. A standard unshaped pulse displays scaling  $\propto \tau_p^{-1}$  and an  $m^{\text{th}}$  order refocusing pulse, appropriately shaped, displays the scaling  $\propto \tau_p^{m+1}$ . Solutions for  $m = 1$  and  $m = 2$  are known [27, 28, 30, 32, 33, 35, 43, 45, 46]. If, however, the autocorrelation of the noise displays a cusp at  $t = 0$ , e.g.,  $\log g(t) \propto -|t|$ , there is *no* pulse shape which makes scaling  $\propto \tau_p^2$  possible. The best possible results is an anomalous scaling  $\propto \tau_p^{3/2}$ . This is the key result of our present work. We will prove it mathematically and illustrate it in simulations.

We stress that our finding is not an academic secondary aspect. The exponential decaying autocorrelation is generic for many processes: For instance, it is characteristic for the omnipresent Ornstein-Uhlenbeck process indicating the slow decay of a quantum state into a continuum of states reaching up to high energies. The best known popular example is radioactive decay. In the context of general spin decoherence we refer the reader to Refs. [51, 52]. After a Fourier transform, an Ornstein-Uhlenbeck noise displays a Lorentzian spectral density. Generally, the cusp of  $g(t)$  at  $t = 0$  yields a slow asymptotic decay  $\propto 1/\omega^2$  for large frequencies. In NMR, noise spectral densities of Lorentzian form are also common [53], leading to homogeneous broadening of the NMR lines. Microscopically, such noise is generated by the fluctuations of dipolar interactions due to random molecular rotations and translations [53]. These rotations are generally very fast. Often, they also imply  $T_1 \approx T_2$ . But in large molecules, e.g., bio-molecules, the time scales can be such that  $T_1 \gg T_2$ . Moreover, we will argue below that the fundamental limits to pulse refocusing are valid also if  $T_1$  and  $T_2$  are of similar magnitude.

The paper is organized as follows: In Sect. 2 the model under study and the ansatz for the shaped pulses is presented. In Sect. 3 a measure for the difference between the real and the ideal pulse is introduced, the Frobenius norm, and the requirements for first- and second-order shaped pulses are derived. In Sect. 4 we report the results of our simulations for an analytical and a cusp-like autocorrelation function. In Sect. 5 we explain why the unexpected 3/2 scaling occurs and prove the no-go theorem for cusp-like autocorrelation functions. Finally, we conclude in

Sect. 6.

## 2. Classical noise systems

We restrict ourselves to pulses in presence of pure dephasing (spin-spin relaxation). This approximation can be used wherever  $T_1 \gg T_2$  holds, for instance in large magnetic fields. The corresponding Hamiltonian reads in the rotating frame

$$H_{\text{tot}} = H(t) + H_p(t) \quad (1a)$$

with the control Hamiltonian

$$H_p(t) = v(t)\sigma_x \quad (1b)$$

and

$$H(t) = \eta(t)\sigma_z \quad (1c)$$

the Hamiltonian for the classical noise. Here we use the term “classical” to indicate that  $\eta(t)$  is a random variable of real numbers obeying a Gaussian distribution. There is no back-action from the spin to the noise and since it couples only to the  $\sigma_z$  operator this coupling commutes with possible drift terms in the Hamiltonian. The Gaussian distribution is defined by its one-point and two-point correlations, i.e., by  $\eta_0(t) = \overline{\eta(t)}$  and by  $g(t_2, t_1) := \overline{\eta(t_2)\eta(t_1)}$ . In addition, it is highly plausible to assume that the bath is translationally invariant in time, i.e., any shift  $t \rightarrow t + \Delta t$  does not alter the noise. This implies that  $\eta_0$  is constant in time and that the autocorrelation  $g(t_2, t_1)$  depends only on the time difference  $g(t_2 - t_1) := g(t_2, t_1)$ . The value of  $\eta_0$  can be seen as an additional magnetic field.

If the random field changes only slowly in time the autocorrelation  $g(t)$  will decay slowly. If it changes quickly  $g(t)$  will decay quickly. If  $\eta(t)$  can change rather abruptly, this corresponds to the influence of noise components at high frequencies. Consequently, the decay in  $g(t)$  displays a singularity at  $t = 0$ .

In the control Hamiltonian,  $v(t)$  stands for the amplitude of the pulse used to rotate the spin around the  $x$  axis. The angle of rotation is given by the time integral of the pulse amplitude

$$\psi(t) := 2 \int_0^t dt' v(t'). \quad (2)$$

The full angle of the pulse is given by  $\psi(\tau_p)$ . For clarity, we consider here spin-flip pulses only with  $\psi(\tau_p) = \pi$ .

The finite duration of the pulse and the non-commutativity of  $H(t)$  and  $H_p(t)$  make the evolution of the combined system non-trivial. We stress, however, that it remains a unitary evolution given by the unitary evolution operator  $U_{\text{tot}}(\tau_p) = \mathcal{T} \exp\{-i \int_0^{\tau_p} H_{\text{tot}}(t) dt\}$ . It cannot be written as the product of the time evolution of the bath alone and the pulse operator  $P_{\tau_p}$ . This form would only hold for an infinitely short pulse because the coupling to the bath would not matter. Formally, one has

$$U_{\text{tot}}(\tau_p) = P_{\tau_p} + \mathcal{O}(\tau_p). \quad (3)$$

A more sophisticated solution consists in shaping the pulse such that the above approximation holds in the form

$$U_{\text{tot}}(\tau_p) = P_{\tau_p} + \mathcal{O}(\tau_p^{m+1}) \quad (4)$$

with integer  $m \geq 0$ . We call such a pulse an  $m$ th-order pulse. Thus, a standard unshaped pulse is a zeroth-order pulse. In this paper, we work with first- and second-order pulses.

The ansatz (4) can be realized for arbitrary  $m$  in principle [35] and concrete proposals have recently been made for second order pulses ( $m = 2$ ) for quantum baths [32, 33]. Furthermore, it could be shown that pulses with this property can be used in pulse sequences if they are not applied at the same instants as instantaneous pulses would be applied, but in adapted sequences [54, 55]. These observations corroborate that the shaping of pulses is an important ingredient for high-fidelity coherent control.

It is not the scope of the present paper to describe how one can find such pulses, see for instance Refs. [25, 27, 28, 32, 33, 37, 45, 46, 55]. Our point here is that the performance of the refocusing pulses depends on the nature of the bath, i.e., on the qualitative form of its autocorrelation function. For illustration, we simulate autocorrelation functions with either a Gaussian or an exponential decay.

### 3. Frobenius norm as measure of pulse quality

The Frobenius norm as such is a way to define a modulus for matrices [56]. It is unbiased in the sense that the Frobenius norm does not depend on the basis in which the matrix is given as long as it is an orthonormal one. We use the Frobenius norm as a measure for the quality of the pulse by applying it to the difference between the density matrix subject to the ideal pulse and the one subject to the real pulse.

We will exploit below that the random dynamics induced by the coupling to classical noise preserves the unitarity of the time evolution so that the Frobenius norm reflects the same behavior as the deviation of a fidelity from unity. Moreover, we will illustrate that the Frobenius norm reflects the behavior of various polarized states so that its behavior is representative for the time evolution of generic initial states.

#### 3.1. General properties

To be specific, we consider the initial density matrices for the completely polarized spin states

$$\rho_0^\alpha = \frac{1 + \sigma^\alpha}{2} \quad (5)$$

where  $\alpha = x, y$  or  $z$  defines the direction of the polarization and  $\sigma^\alpha$  are the Pauli matrices. Next, we let the spin evolve under the evolution operator  $U_{\text{tot}}(\tau_p)$  so that the final density matrices are  $\rho_1^\alpha := U_{\text{tot}}(\tau_p)\rho_0^\alpha U_{\text{tot}}^\dagger(\tau_p)$ . They are compared to the ideal outcomes  $\rho_{\text{id}}^\alpha := P_{\tau_p}\rho_0^\alpha P_{\tau_p}^\dagger$  which have evolved under the perfect pulse  $P_{\tau_p}$ . Thus, we define the Frobenius norm  $\Delta_F$  by

$$\Delta_F^2 := \frac{1}{3} \sum_{\alpha=x,y,z} \text{Tr}(\rho_{\text{id}}^\alpha - \rho_1^\alpha)^2. \quad (6)$$

The sum over the three orthogonal directions is introduced to keep the definition independent from the polarization of the initial state.

Using general properties of density matrices we obtain

$$\Delta_F^2 = 2 \left[ 1 - \frac{1}{3} \sum_{\alpha=x,y,z} \text{Tr}(\rho_{\text{id}}^\alpha \rho_1^\alpha) \right]. \quad (7)$$

Note that the sum in this equation is the fidelity of the real pulse. Its difference to unity yields the Frobenius norm up to a factor of 2. For later use, we define the partial Frobenius norm relevant for the individual directions

$$(\Delta_F^{(\alpha)})^2 := 2 \left[ 1 - \text{Tr}(\rho_{\text{id}}^\alpha \rho_1^\alpha) \right] \quad (8)$$

so that  $\Delta_F^2 = 1/3 \sum_{\alpha=x,y,z} (\Delta_F^{(\alpha)})^2$ .

Further simplification can be achieved by the general ansatz

$$U_{\text{tot}}(\tau_p) = P_{\tau_p} U_c(\tau_p) \quad (9)$$

where all corrections of the real evolution  $U_{\text{tot}}(\tau_p)$  relative to the ideal one  $P_{\tau_p}$  are put into the correcting factor  $U_c(\tau_p)$ . It is given by

$$U_c(\tau_p) = \mathcal{T} \left[ \exp \left( -i \int_0^{\tau_p} \tilde{H}(t) dt \right) \right] \quad (10a)$$

$$\tilde{H}(t) := P_t^\dagger H(t) P_t \quad (10b)$$

where  $P_t$  is the unitary time evolution induced by the control Hamiltonian  $H_p(t)$  alone. As was to be expected, the correcting factor depends solely on the coupling between the spin and the bath. By exploiting the unitarity of  $P_{\tau_p}$  and the properties of the trace, the ideal rotations in  $\Delta_F$  cancel and the Frobenius norm reduces to

$$\Delta_F^2 = 2 - \frac{2}{3} \sum_{\alpha=x,y,z} \text{Tr}(\rho_0^\alpha U_c(\tau_p) \rho_0^\alpha U_c^\dagger(\tau_p)). \quad (11)$$

Inserting the initial states and expanding yields

$$\Delta_F^2 = 1 - \frac{1}{6} \sum_{\alpha=x,y,z} \text{Tr}(\sigma^\alpha U_c(\tau_p) \sigma^\alpha U_c^\dagger(\tau_p)). \quad (12)$$

The correcting factor  $U_c$  is a unitary in the two-dimensional Hilbert space of a spin  $S = 1/2$ . Thus it can always be written as

$$U_c(\tau_p) = \exp(-i\vec{\mu} \cdot \vec{\sigma}). \quad (13)$$

Using Euler's formula this can be expanded yielding

$$U_c(\tau_p) = \cos |\vec{\mu}| - i \frac{\vec{\mu} \cdot \vec{\sigma}}{|\vec{\mu}|} \sin |\vec{\mu}|. \quad (14)$$

Inserting (14) into (12) we obtain

$$\Delta_F^2 = \frac{4}{3} [1 - \cos^2 |\vec{\mu}|]. \quad (15)$$

This simple relation shows that the deviation of the real pulse from the ideal one only depends on the deviation of the correcting unitary  $U_c$  from the identity. No direction in spin space is singled out, i.e., the expression is fully rotationally symmetric in spin space. Since we are mostly interested in the case of small deviations it is sufficient to consider

$$\Delta_F^2 = \frac{4}{3} \vec{\mu}^2 + \mathcal{O}(|\vec{\mu}|^4). \quad (16)$$

### 3.2. Average Hamiltonian theory

The vector  $\vec{\mu}$  can be expressed as the sum  $\vec{\mu} = \sum_{k=1}^{\infty} \vec{\mu}^{(k)}$  resulting of the application of a Magnus expansion [57], see also Ref. [37], to the time-dependent Hamiltonian  $\tilde{H}(t)$  in (10b). Each contribution  $\vec{\mu}^{(k)}$  results from a  $k$ -dimensional integral over  $(k-1)$ -fold nested commutators of  $\tilde{H}(t)$  at different times. So  $\vec{\mu}^{(k)} = O(\tau_p^k)$  holds. The leading terms read

$$\mu_y^{(1)} = \int_0^{\tau_p} dt \eta(t) \sin \psi(t) \quad (17a)$$

$$\mu_z^{(1)} = \int_0^{\tau_p} dt \eta(t) \cos \psi(t). \quad (17b)$$

The non-vanishing second order term is

$$\mu_x^{(2)} = \int_0^{\tau_p} dt_1 \int_0^{t_1} dt_2 \eta(t_1) \eta(t_2) \sin [\psi(t_1) - \psi(t_2)]. \quad (17c)$$

At this stage, one may start expanding  $\eta(t)$  in a Taylor series and trying to make each resulting term vanish. But for a random noise variable this does not make sense. The solution suggesting itself is to discuss the average of the square  $\Delta_F^2$  of the Frobenius norm over random time series  $\eta(t)$ . This is what we will do numerically in the next section in the simulations. In principle, one can also average  $\Delta_F$  instead of the square. We found that this does not make a noticeable difference.

Analytically, we consider here only the leading, first order which becomes

$$\overline{\mu_y^{(1)}} = \eta_0 \int_0^{\tau_p} dt \sin \psi(t) \quad (18a)$$

$$\overline{\mu_z^{(1)}} = \eta_0 \int_0^{\tau_p} dt \cos \psi(t). \quad (18b)$$

Thus, one requires a first-order pulse to fulfill

$$0 = \int_0^{\tau_p} dt \sin \psi(t) \quad (19a)$$

$$0 = \int_0^{\tau_p} dt \cos \psi(t). \quad (19b)$$

Note that these conditions are necessary for a first-order pulse even if  $\eta_0$  vanishes because in the average of  $\Delta_F^2$  the terms  $(\mu_y^{(1)})^2$  and  $(\mu_z^{(1)})^2$  occur as well. Their leading order in  $\tau_p$  is proportional to the variance of  $\eta$  given by  $g(0) > 0$  and to the square of the integrals in (19), see Sect. 5.

## 4. Numerical simulations

We numerically simulated the system of Eq. (1a) with either a Gaussian or an exponential autocorrelation function and for refocusing pulses of different order: The zeroth-order pulse (i.e. a rectangular pulse with constant amplitude), the CORPSE and SCORPSE [27, 28] first-order pulses and three different second-order pulses, CLASS2ND optimized for a classical bath [58] and the pulses SYM2ND and ASYM2ND originally optimized for quantum baths [32]. All these pulses are piecewise

constant  $\pi$ -pulses; their details are given in Appendix A. The discretization of time in the simulation is adapted to represent the switching instants, i.e., the instants at which the amplitude jumps, accurately. For simplicity, we assume that the noise does not have any frequency offset, i.e., the simulations are based on  $\eta_0 = 0$ .

The core part of our simulation program is the sampling of white Gaussian noise that obeys a pre-defined autocorrelation function. For sufficient statistics we need to average over a large number of fluctuations; this requires a random number generator with a very large period. We used the Mersenne Twister generator to sample a large number of discretized fluctuations  $\boldsymbol{\eta} = (\eta_1, \dots, \eta_N)^T$  where  $N$  is the number of time steps  $t_i$ . To this end, we first generate a sequence  $\mathbf{r} = (r_1, \dots, r_N)$  of uncorrelated random numbers obeying Gaussian statistics with vanishing mean value and individual standard deviations  $(\sigma_1, \dots, \sigma_N)^T = (\text{diag } \mathbf{D})$ . The diagonal matrix  $\mathbf{D}$  is given by the eigen decomposition  $\mathbf{G} = \mathbf{O} \mathbf{D} \mathbf{O}^T$  of the covariance matrix  $(\mathbf{G})_{ij} = g(t_i - t_j)$  of the random fluctuations  $\eta(t)$ . Finally, the vector  $\mathbf{r}$  is transformed to the non-diagonal basis  $\boldsymbol{\eta} = \mathbf{O} \mathbf{r}$  to obtain the correlated Gaussian noise  $\boldsymbol{\eta}$ .

Since we are dealing with a two-level system, the numerical integration is carried out easily for arbitrary pulses. A reduction of the integration error for time-dependent Hamiltonians is achieved by commutator-free exponential time propagators (CFETs) as introduced by Alvermann *et al.* [59, 60]. The additional numerical effort is negligible because an exact analytical representation of the time-evolution operator of a two-level system is available. Hence, no additional diagonalizations are induced by the CFETs.

We render the results of our simulations as functions of  $1/v$ , where  $v$  denotes the maximum amplitude of the pulse. This choice respects the scenario relevant for experiments because generically the constraint is on the maximum realizable amplitude, not on the duration  $\tau_p$  of the pulse. Thus, a simple pulse, though of low order, may be experimentally advantageous because it is shorter. This feature is taken into account by the plots against  $1/v$ . We point out that for a given constant amplitude different  $\pi$ -pulses will be of different durations  $\tau_p$ . But for the same pulse shape  $\tau_p \propto 1/v$  holds so that the same scaling is observed.

### 4.1. Noise with Gaussian autocorrelation

We consider a bath with the Gaussian autocorrelation function

$$g(t) = g_0^2 e^{-\gamma^2 t^2}, \quad (20)$$

where  $g(0) = g_0^2$  determines the energy scale of the system while  $\gamma$  sets the decay rate of the correlation.

In Fig. 1, we illustrate how the total Frobenius norm is composed of its partial contributions. The figure exemplarily show the results for the partial contributions to the Frobenius norm (8) for the SCORPSE pulse. The central message of Fig. 1 is that all three contributions display the *same* scaling behavior  $\propto \tau_p^2 \propto 1/v^2$ . Thus the total Frobenius norm follows the same scaling and there is no need to consider the partial contributions separately. Otherwise, one should discuss the full map of the real pulse as in quantum tomography.



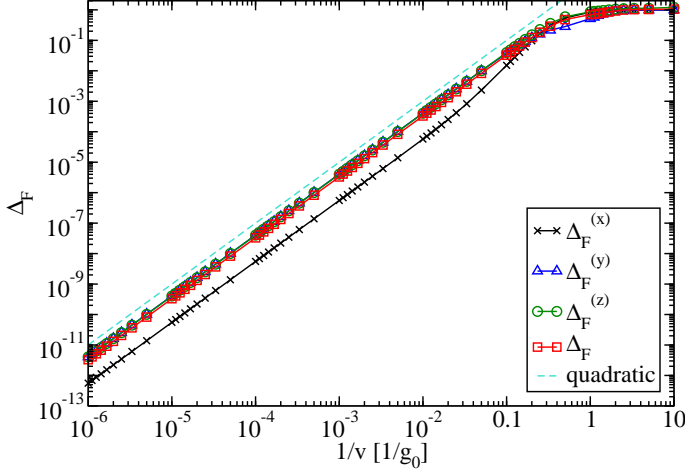


Figure 1: Frobenius norm  $\Delta_F$  for a SCORPSE pulse and the individual contributions  $\Delta_F^{(\alpha)}$  defined in Eq. (8) from  $\rho^\alpha$ ,  $\alpha \in \{x, y, z\}$  versus the inverse pulse amplitude  $1/v$ . The autocorrelation function is given in Eq. (20) with  $\gamma = 0.1 g_0$ .

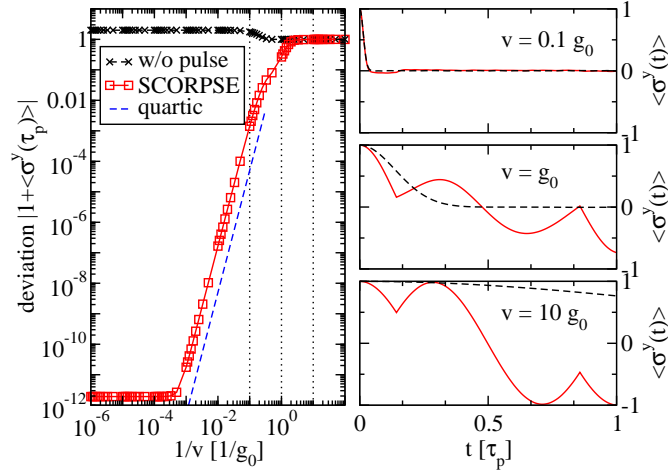


Figure 2: Deviation of the polarization  $\langle \sigma^y(\tau_p) \rangle$  from its ideal value  $\langle \sigma^y(\tau_p) \rangle = -1$  after the application of the SCORPSE pulse as a function of the inverse pulse amplitude  $1/v$  (left panel). In the right panel, the polarization  $\langle \sigma^y(t) \rangle$  in the course of the SCORPSE pulse is plotted for three different values of the pulse amplitude  $v$ . The noise follows the autocorrelation (20) with  $\gamma = 0.1 g_0$ .

Fig. 2 illustrates the detailed analysis of a particular polarization. The right panels show the temporal evolution of the  $y$ -polarization during the pulse. Due to the spin flip around  $\sigma^x$  it is eventually negated. How well this is achieved depends on the duration  $\tau_p$  of the pulse or, putting the same in a different way, on the inverse amplitude  $1/v$ . For larger amplitude the wanted value  $\langle \sigma^y(\tau_p) \rangle = -1$  is achieved better than for lower values. This fact is summarized in the left panel where also the quartic scaling is shown. This quartic power law is the direct consequence of the scaling  $\Delta_F \propto \tau_p^2$  because for a  $\pi$ -pulse a small error  $\Delta\psi$  in the spin flip angle  $\psi(\tau_p)$  implies a deviation  $\propto (\Delta\psi)^2$ . Thus, the deviation  $|1 + \langle \sigma^y(\tau_p) \rangle|$  scales like  $\Delta_F^2 \propto \tau_p^4 \propto 1/v^4$ . The key point is again that the relevant scaling feature is represented by the total Frobenius norm  $\Delta_F$ .

On the basis of the above considerations we are now in the position to compare the scaling of  $\Delta_F$  of different pulses, knowing that this measure represents the performance of the

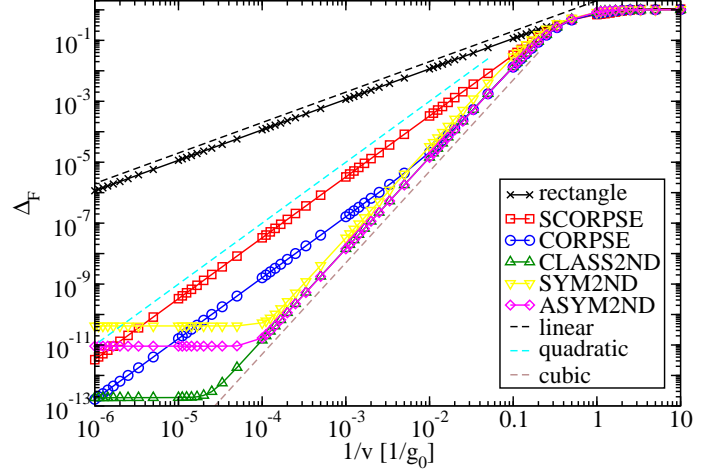


Figure 3: Frobenius norm  $\Delta_F$  versus the inverse pulse amplitude  $1/v$  for various pulses, see legend. For comparison, various power laws are depicted as dashed lines. The autocorrelation is Gaussian, see Eq. (20), with  $\gamma = 0.1 g_0$ . The simulation was carried out for 500,000 random configurations  $\eta(t)$ .

pulses. We do so in Fig. 3. The pulses are given in detail in Appendix A. It is obvious that they obey significantly different scalings. As expected, the standard rectangular pulse displays linear scaling. The first-order pulses SCORPSE and CORPSE indeed display the quadratic scaling. It is remarkable, that the CORPSE pulse does even better in a certain transition region of larger values  $1/v$ . There it behaves like a second-order pulse with cubic scaling down till  $1/v \approx 10^{-2}/g_0$ , where the exponent switches to quadratic behavior. The second-order pulses by design (CLASS2ND, SYM2ND, ASYM2ND) display the proper cubic scaling. They behave very similarly so that from this simulation none of them is to be preferred over the others.

At very low values of  $1/v$  and thus of  $\Delta_F \approx 10^{-12}$  plateaus appear for the more complicated pulses. This is a direct effect of numerical inaccuracies in the simulations or in the representation of the pulses. For lower accuracies, the plateaus would appear at larger values of  $\Delta_F$ . For theoretical clarity, we used the high-precision data for the pulses given in Appendix A. This allows us to show the asymptotic power laws very clearly. Of course, in experiment a lower accuracy in the realization of the pulses will lead to plateau-like behavior for larger  $\Delta_F$ . We observe linear scaling between the pulse accuracy and the plateau of  $\Delta_F$ , this means, that a  $10^{-3}$  accuracy in the pulse realization will roughly imply that the power law in the pulse performance is cut off at  $\Delta_F \approx 10^{-3}$  and so on.

The key message of Fig. 3 is that the simulations confirm the expected analytical behavior for which the pulses were designed. An  $m$ -th order pulse indeed shows scaling  $\propto \tau_p^{m+1} \propto 1/v^{m+1}$ . This is established exemplarily for  $m = 0, 1, 2$ .

#### 4.2. Noise with exponential autocorrelation

We study the exponentially decaying autocorrelation function

$$g(t) = g_0^2 e^{-\gamma|t|}. \quad (21)$$

The main difference to the Gaussian autocorrelation simulated in the previous subsection is the cusp at  $t = 0$ .

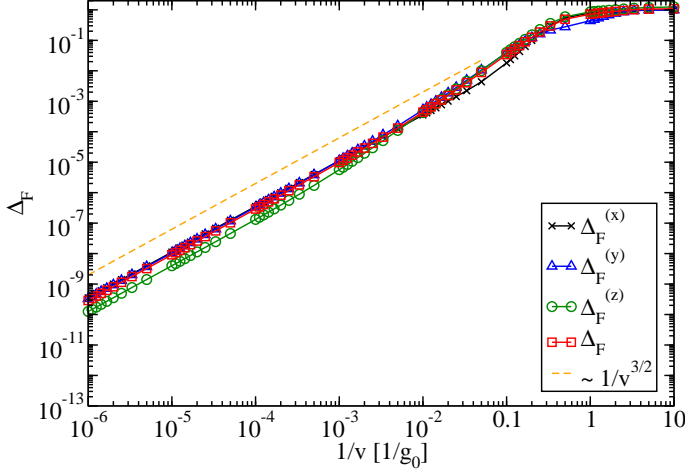


Figure 4: Frobenius norm  $\Delta_F$  for a SCORPSE pulse and the individual contributions  $\Delta_F^{(\alpha)}$  defined in Eq. (8) from  $\rho^\alpha$ ,  $\alpha \in \{x, y, z\}$  versus the inverse pulse amplitude  $1/v$ . The autocorrelation function is given in Eq. (21) with  $\gamma = 0.01 g_0$ .

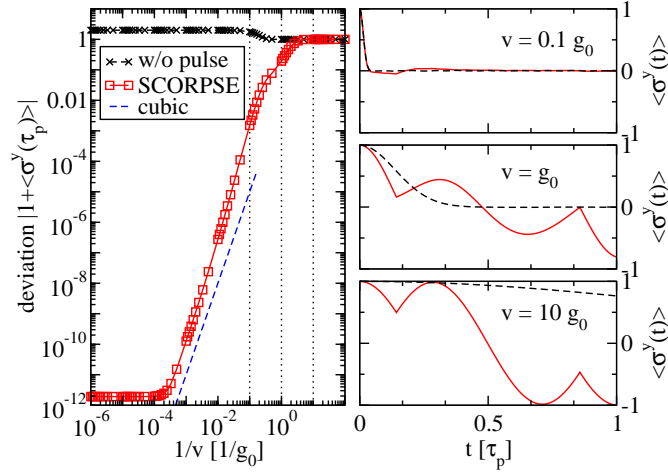


Figure 5: Deviation of the polarization  $\langle \sigma^y(\tau_p) \rangle$  from its ideal value  $\langle \sigma^y(\tau_p) \rangle = -1$  after the application of the SCORPSE pulse as a function of the inverse pulse amplitude  $1/v$  (left panel). In the right panel, the polarization  $\langle \sigma^y(t) \rangle$  in the course of the SCORPSE pulse is plotted for three different values of the pulse amplitude  $v$ . The noise follows the autocorrelation (21) with  $\gamma = 0.01 g_0$ .

First, we show as before that the partial contributions along the three directions behave the same in the sense that they display the same scaling, see Fig. 4. The precise form of the scaling is indeed anomalous displaying the proportionality  $\propto \tau_p^{3/2} \propto 1/v^{3/2}$ . We will come back to this point below. Similarly, we confirm that the Frobenius norm is representative for the behavior of the polarization, see Fig. 5. The scaling observed in the left panel is consistent with the scaling observed in Fig. 4, but it differs from what we found for the analytic autocorrelation in the previous subsection.

Fig. 6 summarizes the comparison of the simulations of  $\Delta_F$  of various pulses. The unshaped rectangular pulse behaves linearly as expected. All pulses of first and second order reveal a rather surprising behavior expressed by the scaling  $\Delta_F \propto 1/v^{3/2}$  involving the unexpected half-integer value  $3/2$  for the scaling exponent. Power-laws with exponents larger than  $3/2$  can be discerned for very limited regions of larger values of  $1/v$ .

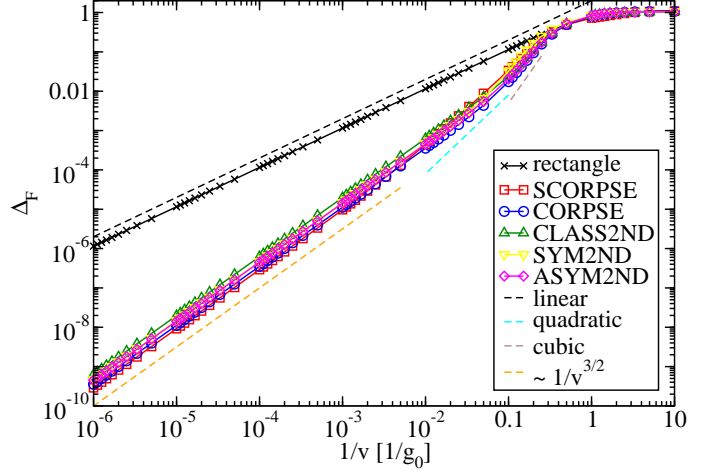


Figure 6: Frobenius norm  $\Delta_F$  versus the inverse pulse amplitude  $1/v$  for various pulses, see legend. For comparison, various power laws are depicted as dashed lines. The autocorrelation is an exponential, see Eq. (21), with  $\gamma = 0.01 g_0$ . The simulation was carried out for 500,000 random configurations  $\eta(t)$ .

For faster decaying autocorrelations, i.e.  $\gamma > 0.01 g_0$ , these regions vanish completely and  $\Delta_F \propto 1/v^{3/2}$  is the only identifiable power law. Thus, it is detectable also for an accuracy of, e.g.,  $10^{-3}$ .

To our knowledge, the occurrence of half-integer exponents in the scaling of pulse performance is a unique feature which has not been mentioned in the literature so far. Similarly, we stress that it is remarkable that the first- and the second-order pulses behave almost alike in striking contrast to what can be observed for the Gaussian autocorrelation in Fig. 3. It bears an important implication for experiment because it sets strict limits to what can be achieved by pulse design.

Of course, it is important to understand the origin of this unexpected and anomalous scaling. It is plausible to attribute it to the singularity in the autocorrelation. This view is supported by a similar observation made recently in the analysis of sequences of ideal pulses [14, 15, 17, 18, 61].

## 5. Scaling due to singular autocorrelation

In view of the general framework developed in Sect. 3 we know that we have to consider the average of  $\vec{\mu}^2$  over the random configurations  $\eta(t)$ , see Eq. (16). The Magnus expansion, see Subsect. 3.2, helps us to identify the leading contributions in an expansion in powers of  $\tau_p$ . For instance, it is obvious that  $\mu_x^{(2)}$  in Eq. (17c) contributes to the average of  $\Delta_F^2$  only in order  $\tau_p^4$  because  $\mu_x^{(2)} \propto \tau_p^2$  due to the double integral. Thus the only candidate for contributions of lower order is

$$\overline{(\mu_y^{(1)})^2} + \overline{(\mu_z^{(1)})^2} = \int_0^{\tau_p} dt_1 \int_0^{\tau_p} dt_2 g(t_1 - t_2) \cos[\psi(t_1) - \psi(t_2)] \quad (22)$$

which follows from the definition (17) and the appropriate trigonometric relation.

To understand the behavior of the expression on the right hand side of (22) we use an expansion of the autocorrelation around  $t = 0$

$$g(t) = g_0^2 - g_1^2 \gamma |t| + O(t^2). \quad (23)$$

Inserting the leading order of this expansion in the integral of Eq. (22) yields

$$I_1 := g_0^2 \int_0^{\tau_p} dt_1 \int_0^{\tau_p} dt_2 \cos[\psi(t_1) - \psi(t_2)] \quad (24a)$$

$$= g_0^2 \left[ \int_0^{\tau_p} dt \cos \psi(t) \right]^2 + g_0^2 \left[ \int_0^{\tau_p} dt \sin \psi(t) \right]^2 \quad (24b)$$

which implies  $\Delta_F^2 = \frac{4}{3}(I_1 + \text{higher orders})$ . Clearly, this contribution vanishes if the condition (19) is fulfilled. This means that this contribution vanishes for any first-order pulse. This is perfectly consistent since  $I_1$  would scale  $\propto \tau_p^2$  if it is non-vanishing so that  $\Delta_F \propto \tau_p$  would ensue.

Next, we consider the linear order in the expansion Eq. (22) yielding

$$I_{3/2} = -g_1^2 \gamma \int_0^{\tau_p} dt_1 \int_0^{\tau_p} dt_2 |t_1 - t_2| \cos[\psi(t_1) - \psi(t_2)]. \quad (25)$$

Clearly, this term scales like  $I_{3/2} \propto \tau_p^3 \propto 1/\nu^3$  so that it readily explains the occurrence of  $\Delta_F^2 \propto 1/\nu^3$  implying  $\Delta_F \propto 1/\nu^{3/2}$  naturally. Therefore, the origin of the  $3/2$  behaviour of the Frobenius norm has been identified. A quantitative check of the prefactor in the scaling is carried out for the SCORPSE and the CORPSE pulse in Appendix B. The quantitative agreement found supports our conclusion.

We underline that the contribution  $I_{3/2}$  does not occur if the autocorrelation  $g(t)$  is assumed to be analytical. Since  $g(t) = g(-t)$  holds by definition, the analyticity prevents odd powers of  $t$  to occur. Then, no finite  $g_1$  term occurs in the expansion (23) and thus no  $I_{3/2}$  can arise. The next-leading contribution would be a term  $I_2 \propto \tau_p^4$ .

We point out that the occurrence of  $I_{3/2}$  due to the singularity of the autocorrelation at  $t = 0$  does not rely on the particular angle of rotation studied, here  $\pi$ -pulses. Thus we expect that qualitatively the same feature occurs for any control pulse.

In view of the above results one has to wonder whether we tried inappropriate pulses and whether it is not possible to make  $I_{3/2}$  vanish by appropriate design of the pulse. Indeed, we tried to find pulses also fulfilling  $I_{3/2} = 0$  besides the first-order conditions (19). But we failed to find such solutions. Instead we realized that it is rigorously impossible that such pulses exist. We prove in Appendix C that the two standard first-order conditions (19) implying  $I_1 = 0$  and the additional condition  $I_{3/2} = 0$  cannot be fulfilled simultaneously. Note that this naturally explains why all the pulses whose performance is simulated in Fig. 6 behave qualitatively the same, i.e., displaying the same exponent, except for the non-refocusing rectangular pulse.

This is a strict no-go statement relevant for refocusing pulses in presence of classical noise with a autocorrelation function with a cusp at  $t = 0$ . As a consequence, pulses designed for

this kind of noise should be optimized in such a way that  $I_{3/2}$  is minimized under the constraint that the standard integrals (19) vanish. Then, the detrimental influence of the half-integer contribution  $\Delta_F \propto 1/\nu^{3/2}$  is reduced to its theoretical minimum.

We expect that this finding extends to noises with weaker singularities. For instance, a singularity  $\ln(g(t)) \propto |t|^3$  implies high-frequency tails  $\propto 1/\omega^4$ . Note that recent spin noise measurements indeed revealed tails with exponents  $\propto 1/\omega^{3.6}$  [62] for the noise experienced by the  $^{13}\text{C}$  spins in adamantane. We presume that such noise induces non-vanishing terms  $I_{5/2}$  which imply scaling exponents of  $5/2$ .

We point out that the fundamental limit for improving pulses applies also to the case where  $T_1$  and  $T_2$  do not differ substantially, e.g., in liquid NMR. This is so because an *additional* coupling to the noise clearly complicates the task to construct a refocusing pulse. Indeed, additional constraints have to be fulfilled by the pulses in linear and any higher order, see Ref. [58]. But because the reduced set of equations for the pure dephasing case with  $T_1 = \infty$  does not have a solution as proven here, no extended set will have a solution either.

Nevertheless, further studies of more specific models are called for, for instance, it has to be elucidated how the widespread case of spectral densities between Lorentzian and Gaussian shape [63, 64] influence the possibility to construct efficient refocusing pulses.

## 6. Conclusions

In this paper, we have studied a spin  $S = 1/2$  subject to random dephasing due to classical noise of Gaussian statistics. We numerically simulated and analytically analysed the performance of various spin-flip pulses. To this end, we have introduced a mathematically clearly defined measure for the quality of the pulses, namely the Frobenius norm  $\Delta_F$  of the difference between the ideal outcome of an ideal pulse and the real outcome of the real pulse of finite duration. The Frobenius norm is closely related to the fidelity.

The aim was to show how pulses shaped to refocus the detrimental dephasing perform and that this can be seen in the scaling of  $\Delta_F$  with the pulse duration  $\tau_p$ . A standard rectangular pulse shows  $\Delta_F \propto \tau_p$ , a first-order pulse  $\Delta_F \propto \tau_p^2$ , a second-order pulse  $\Delta_F \propto \tau_p^3$ , and so on. This could indeed be verified in the simulations assuming noise with analytical autocorrelation  $g(t)$ . But the simulation of noise with singular autocorrelation displayed unexpected behavior. Such autocorrelations are generic for Ornstein-Uhlenbeck processes, that means for systems with spectral densities of Lorentzian shape. We simulated a process which is governed by  $g(t) \propto \exp(-\gamma|t|)$ , i.e., with a cusp at  $t = 0$ . The pulse shaping does not improve the scaling beyond first order. All refocusing pulses, i.e., shaped pulses beyond the rectangular pulses, display anomalous scaling  $\Delta_F \propto \tau_p^{3/2}$ .

We have clarified analytically that the anomalous scaling stems from the cusp at  $t = 0$ . It could be rigorously proven that no pulse design can avoid the anomalous scaling.

We stress that a cusp at  $t = 0$  is not just a mathematical peculiarity because the cusp is generated by the coupling to high-frequency fluctuations. Thus, the deeper physical reason for the impossibility to improve the pulse performance by shaping is that infinitely fast fluctuations contribute to the noise. They are manifest in the spectral density of cusp-like autocorrelations displaying high-frequency tails  $\propto 1/\omega^2$  which do not converge quickly, i.e., exponentially, to zero. Similar findings have been made before in the analysis in the design of sequences of ideal pulses [14, 15, 17, 18, 61]. The sequences could not be improved beyond a certain scaling if the power spectrum of the noise displayed soft high-frequency cutoffs following power laws.

We stress that processes with cusps in the autocorrelation function are common in nature. For instance, the exponential autocorrelation belongs to Ornstein-Uhlenbeck noise which is observed wherever a slow decay into a continuum of states without high-energy cutoff occurs. Note that on the frequency scale of microwaves already translational and rotational motion takes place fast, i.e., on practically infinitesimally short time scales. Thus the coupling to such degrees of freedom induces homogeneous broadening with Lorentzian spectral density [53].

Summarizing, the results reported here imply an important general message which is largely independent of the details of the system: There are fundamental limits to pulse refocusing if the noise comprises significant high-frequency components. We investigated the simplest model where this phenomenon occurs so that the effect is not obscured by complexity. Thus we restricted ourselves to  $T_1 = \infty$  considering only spin-spin relaxation. But our conclusions apply also to the case where  $T_1$  and  $T_2$  are comparable because the inclusion of additional couplings to random noise increases the number of constraints to be fulfilled by refocusing pulses. Hence the impossibility of higher order refocusing pulses for infinite  $T_1$  implies the impossibility of such pulses for finite  $T_1$ .

These observations may be seen as bad news, but there is also some good news for the analysis of noise. If anomalous scaling is found in the performance of refocusing pulses one can deduce that the noise is characterized by singular autocorrelations. These observations should be of use in a large variety of NMR experiments.

## 7. Acknowledgements

We are thankful to Roland Böhmer and Dieter Suter for helpful discussions on relaxation mechanisms in NMR. We acknowledge financial support by the Studienstiftung des deutschen Volkes (DS) and by the DFG in project UH 90/9-1 (GSU).

## Appendix A. Piecewise constant pulses

Here we present the details of the  $\pi$ -pulses simulated in Sect. 4. All pulses are piecewise constant and rotate the spin around the  $\sigma^x$ -axis or any other fixed axis in the  $\sigma^x\sigma^y$ -plane. The investigated pulses comprise the symmetric SCORPSE and the

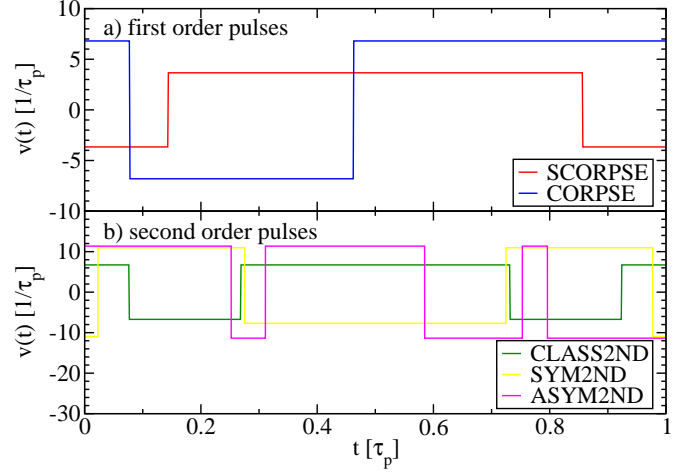


Figure A.7: Pulse amplitude  $v(t)$  versus time  $t$ . The first-order  $\pi$ -pulses are the symmetric SCORPSE and asymmetric CORPSE pulse [27, 28]. In second order, a  $\pi$ -pulse (CLASS2ND) derived for a classical bath [58] and the quantum mechanical symmetric SYM2ND and asymmetric ASYM2ND  $\pi$ -pulses [32] are presented.

asymmetric CORPSE pulse [27, 28] which are both first-order pulses. Furthermore, a second-order pulse (CLASS2ND) derived for a classical bath [58] is studied. In addition, we discuss the second-order symmetric SYM2ND and the asymmetric ASYM2ND pulses derived in Ref. [32] where the bath was treated on the quantum level.

The time dependence of the pulse amplitudes  $v(t)$  is plotted in Fig. A.7, while the corresponding switching instances  $\tau_i$ , at which the amplitudes jump, and their values  $v_{\tau_i}$  are listed in Tab. A.1.

The parameters of the second-order pulses in Tab. A.1 are given in the same high precision as used in our numerical simulation. This allows us to illustrate the power law scaling down to very small values of  $1/\nu$  and of  $\Delta_F$ . If the accuracy in a simulation or in an experimental realization is lower the power laws are cut off on the scale of the accuracy, see plateaus in Fig. 3 for illustration. This means that plateaus occur at values  $\Delta_F$  of the order of the accuracy. For instance, if the accuracy is say  $10^{-2}$ ,  $\Delta_F$  will not fall below about  $10^{-2}$ , if the accuracy is  $10^{-3}$ ,  $\Delta_F$  will form a plateau at about  $10^{-3}$ .

## Appendix B. Quantitative check of the anomalous scaling

In Sect. 5, the analytic expression (25) for  $I_{3/2}$  has been derived which explains the anomalous scaling  $\Delta_F \propto \tau_p^{3/2} \propto 1/\nu^{3/2}$ . To be sure that this is the complete explanation we here check  $\Delta_F^2 = (4/3)I_{3/2} + \mathcal{O}(\tau_p^4)$  quantitatively for some pulses. The following explicit results apply to the first-order CORPSE and SCORPSE pulse, but the extension to other pulses is straightforward.

In order to check  $\Delta_F^2 = (4/3)I_{3/2}$ , we have to carry out the integrals in Eq. (25). The evaluation for the individual pulses is straightforward, but rather lengthy. We only give a short description of the procedure and present the results. One has to evaluate the time-dependent angle  $\psi(t) = 2 \int_0^t dt' v(t')$  which for



| $\nu_{\tau_i} [1/\tau_p]$  | $\tau_i [\tau_p]$    |
|----------------------------|----------------------|
| <b>SCORPSE</b>             |                      |
| $\pm \frac{7\pi}{6}$       | $\frac{1}{7}$        |
|                            | $\frac{6}{7}$        |
| <b>CORPSE</b>              |                      |
| $\pm \frac{13\pi}{6}$      | $\frac{1}{13}$       |
|                            | $\frac{6}{13}$       |
| <b>CLASS2ND</b>            |                      |
| $\pm 6.72572865242397$     | $0.07623077665509$   |
|                            | $0.26784318744464$   |
|                            | $0.73215681255536$   |
|                            | $0.92376922334491$   |
| <b>SYM2ND</b>              |                      |
| $\pm 10.95012043866828575$ | $0.0228054551625108$ |
| $-7.69537638364247465$     | $0.2752692173069500$ |
|                            | $0.7247307826930500$ |
|                            | $0.9771945448374892$ |
| <b>ASYM2ND</b>             |                      |
| $\pm 11.36443379447147705$ | $0.2520112376736856$ |
|                            | $0.3108959015038718$ |
|                            | $0.5847810746672190$ |
|                            | $0.7528254671237393$ |
|                            | $0.7960392449336322$ |

Table A.1: Amplitudes  $\nu_{\tau_i}$  and switching instances  $\tau_i$  of the first- and second-order  $\pi$ -pulses used in the numerical simulations. The resulting amplitudes  $\nu(t)$  are plotted in Fig. A.7.

the first-order CORPSE and SCORPSE pulses reads

$$\psi_{\text{CORPSE}}(t) = \begin{cases} \frac{13\pi}{3} \cdot t & 0 \leq t \leq \frac{\tau_p}{13} \\ \frac{2\pi}{3} - \frac{13\pi}{3\tau_p} \cdot t & \frac{\tau_p}{13} < t \leq \frac{6\tau_p}{13} \\ -\frac{10\pi}{3} + \frac{13\pi}{3\tau_p} \cdot t & \frac{6\tau_p}{13} < t \leq \tau_p \end{cases} \quad (\text{B.1a})$$

and

$$\psi_{\text{SCORPSE}}(t) = \begin{cases} -\frac{7\pi}{3\tau_p} \cdot t & 0 \leq t \leq \frac{\tau_p}{7} \\ -\frac{2\pi}{3} + \frac{7\pi}{3\tau_p} \cdot t & \frac{\tau_p}{7} < t \leq \frac{6\tau_p}{7} \\ \frac{10\pi}{3} - \frac{7\pi}{3\tau_p} \cdot t & \frac{6\tau_p}{7} < t \leq \tau_p \end{cases}, \quad (\text{B.2a})$$

respectively. Inserting these expressions in Eq. (25) allows us to carry out the two-dimensional integration analytically. Finally, this yields the power laws

$$\Delta_F^2|_{\text{CORPSE}} = 4\pi g_0^2 \gamma \left(\frac{1}{\nu}\right)^3 \quad (\text{B.3a})$$

$$\Delta_F^2|_{\text{SCORPSE}} = \frac{8\pi}{3} g_0^2 \gamma \left(\frac{1}{\nu}\right)^3 \quad (\text{B.3b})$$

for the leading order of the Frobenius norm  $\Delta_F$ . In Fig. B.8, these power laws (dashed lines) are compared with the numerical results from simulation. For both pulses and all values

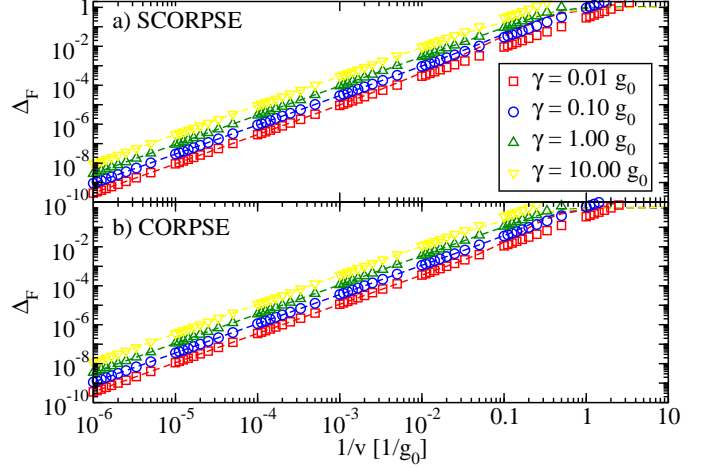


Figure B.8: Frobenius norm  $\Delta_F$  versus the inverse pulse amplitude  $1/\nu$  for the autocorrelation  $g(t) = g_0^2 e^{-\gamma|t|}$ . The analytic results (dashed lines) quantitatively explain the unexpected  $\Delta_F \propto 1/\nu^{3/2}$  behavior including the prefactor. The numerical results are depicted by the symbols. Note that there is no fit involved.

of  $\gamma$ , the agreement is perfect. Hence, the anomalous scaling  $\Delta_F \propto 1/\nu^{3/2}$  can indeed be attributed to the contribution  $I_{3/2}$  given in Eq. (25).

### Appendix C. Proof of the no-go theorem

Here we prove that  $I_1$  in Eq. (24b) and  $I_{3/2}$  in Eq. (25) cannot be made vanish simultaneously. To this end, we rewrite

$$I_{3/2} = -aI_{3/2}^a - aI_{3/2}^b \quad (\text{C.1a})$$

$$I_{3/2}^a = \int_0^{\tau_p} dt_1 \int_0^{\tau_p} dt_2 \cos \psi_1 |t_1 - t_2| \cos \psi_2 \quad (\text{C.1b})$$

$$I_{3/2}^b = \int_0^{\tau_p} dt_1 \int_0^{\tau_p} dt_2 \sin \psi_1 |t_1 - t_2| \sin \psi_2, \quad (\text{C.1c})$$

where  $a = g_0^2 \gamma$  and we have abbreviated  $\psi_i := \psi(t_i)$  for brevity. In the Hilbert space  $\mathcal{H}$  of real integrable functions in the time interval  $[0, \tau_p]$  both integrals can be interpreted as expectation values

$$I_{3/2}^a = \langle \cos(\psi) | A | \cos(\psi) \rangle \quad (\text{C.2a})$$

$$I_{3/2}^b = \langle \sin(\psi) | A | \sin(\psi) \rangle \quad (\text{C.2b})$$

of the linear operator  $A$  with the matrix elements  $|t_1 - t_2|$ . The corresponding mapping of the function  $\varphi(t) \in \mathcal{H}$  to the function  $\psi(t)$  reads

$$A : \varphi(t) \mapsto \psi(t) = \int_0^{\tau_p} dt' A(t, t') \varphi(t'). \quad (\text{C.3})$$

The idea is to write the operator  $A$  in a form containing  $B^\dagger B$  because this implies that  $I_{3/2}$  is non-negative. An educated

guess for an absolute value is the sign function because it is the derivative of the absolute value function. Thus we consider

$$B : \varphi(t) \mapsto \psi(t) = \int_0^{\tau_p} dt' \operatorname{sgn}(t-t')\varphi(t'). \quad (\text{C.4})$$

Obviously, this operator is antihermitian, i.e.,  $B^\dagger = -B$ . We compute the square  $B^2$

$$B^2 : \varphi(t) \mapsto \chi(t) = \int_0^{\tau_p} dt_1 \int_0^{\tau_p} dt_2 \operatorname{sgn}(t-t_1) \times \operatorname{sgn}(t_1-t_2)\varphi(t_2). \quad (\text{C.5})$$

The integration with respect to  $t_1$  can be carried out analytically leading to

$$B^2 : \varphi(t) \mapsto \chi(t) = \int_0^{\tau_p} dt_2 (2|t-t_2| - 1) \varphi(t_2). \quad (\text{C.6})$$

Indeed, this establishes a relation between  $A$  and  $B^2 = -B^\dagger B$  which reads

$$A = \frac{1}{2} (C - B^\dagger B) \quad (\text{C.7})$$

where we used  $B = -B^\dagger$  and introduced the operator

$$C : \varphi(t) \mapsto \psi(t) = \int_0^{\tau_p} dt' \varphi(t'). \quad (\text{C.8})$$

Next, we observe that a pulse with  $\psi(t)$  which fulfills the first-order condition (19) automatically obeys

$$0 = C|\sin(\psi)\rangle \quad (\text{C.9a})$$

$$0 = C|\cos(\psi)\rangle. \quad (\text{C.9b})$$

Thus, in the subspace of first-order pulses the relations

$$I_{3/2}^a = -\frac{1}{2} \langle B \cos(\psi) | B \cos(\psi) \rangle \leq 0 \quad (\text{C.10a})$$

$$I_{3/2}^b = -\frac{1}{2} \langle B \sin(\psi) | B \sin(\psi) \rangle \leq 0 \quad (\text{C.10b})$$

$$I_{3/2} = \frac{a}{2} (\langle B \cos(\psi) | B \cos(\psi) \rangle + \langle B \sin(\psi) | B \sin(\psi) \rangle) \geq 0 \quad (\text{C.10c})$$

hold demonstrating the non-negativity of the anomalous contribution. Hence  $I_{3/2} = 0$  implies that  $0 = B|\cos(\psi)\rangle = B|\sin(\psi)\rangle$ . Functions  $\varphi(t) = \cos(\psi(t))$  or  $\varphi(t) = \sin(\psi(t))$  which are annihilated by the mapping  $B$  fulfill

$$0 = \int_0^{\tau_p} dt' \operatorname{sgn}(t-t')\varphi(t') \quad (\text{C.11})$$

for all values of  $t$ . Taking the derivative with respect to  $t$  on both sides implies

$$0 = 2 \int_0^{\tau_p} dt' \delta(t-t')\varphi(t') = 2\varphi(t) \quad (\text{C.12})$$

so that  $\varphi(t)$  has to vanish for all  $t$ . No such solution exists for  $\psi(\tau_p) - \psi(0) = \pi$ . We conclude that it is impossible to make  $I_1$  and  $I_{3/2}$  zero simultaneously.

As a consequence, pulses designed for Ornstein-Uhlenbeck noise can only be optimized in such a way that  $I_1 = 0$ , see Eq. (19), and that  $I_{3/2}$  is minimized. This is the best one can aim for.

## References

- [1] E. L. Hahn, Spin echoes, Phys. Rev. 80 (1950) 580.
- [2] H. Y. Carr, E. M. Purcell, Effects of diffusion on free precession in nuclear magnetic resonance experiments, Phys. Rev. 94 (1954) 630.
- [3] S. Meiboom, D. Gill, Modified spin-echo method for measuring nuclear relaxation times, Rev. Sci. Instr. 29 (1958) 688.
- [4] U. Haeberlen, High Resolution NMR in Solids: Selective Averaging, Academic Press, New York, 1976.
- [5] A. A. Maudsley, Modified Carr-Purcell-Meiboom-Gill sequence for NMR Fourier imaging applications, J. Mag. Res. 69 (1986) 488.
- [6] T. Gullion, D. B. Baker, M. S. Conradi, New, compensated Carr-Purcell sequences, J. Mag. Res. 89 (1990) 479.
- [7] M. H. Levitt, Spin Dynamics, Basics of Nuclear Magnetic Resonance, John Wiley & Sons, Ltd, Chichester, 2005.
- [8] L. Viola, S. Lloyd, Dynamical suppression of decoherence in two-state quantum systems, Phys. Rev. A 58 (1998) 2733.
- [9] M. Ban, Photon-echo technique for reducing the decoherence of a quantum bit, J. Mod. Opt. 45 (1998) 2315.
- [10] L. Viola, E. Knill, S. Lloyd, Dynamical decoupling of open quantum systems, Phys. Rev. Lett. 82 (1999) 2417.
- [11] K. Khodjasteh, D. A. Lidar, Performance of deterministic dynamical decoupling schemes: Concatenated and periodic pulse sequences, Phys. Rev. A 75 (2007) 062310.
- [12] G. S. Uhrig, Keeping a quantum bit alive by optimized  $\pi$ -pulse sequences, Phys. Rev. Lett. 98 (2007) 100504.
- [13] G. S. Uhrig, Erratum: Keeping a quantum bit alive by optimized  $\pi$ -pulse sequences, Phys. Rev. Lett. 106 (2011) 129901.
- [14] G. S. Uhrig, Exact results on dynamical decoupling by  $\pi$ -pulses in quantum information processes, New J. Phys. 10 (2008) 083024.
- [15] G. S. Uhrig, Corrigendum: Exact results on dynamical decoupling by  $\pi$ -pulses in quantum information processes, New J. Phys. 13 (2011) 059504.
- [16] W. Yang, R.-B. Liu, Universality of Uhrig dynamical decoupling for suppressing qubit pure dephasing and relaxation, Phys. Rev. Lett. 101 (2008) 180403.
- [17] L. Cywiński, R. M. Lutchyn, C. P. Nave, S. Das Sarma, How to enhance dephasing time in superconducting qubits, Phys. Rev. B 77 (2008) 174509.
- [18] S. Pasini, G. S. Uhrig, Optimized dynamical decoupling for power-law noise, Phys. Rev. A 81 (2010) 012309.
- [19] A. Ajoy, G. A. Álvarez, D. Suter, Optimal pulse spacing for dynamical decoupling in the presence of a purely dephasing spin bath, Phys. Rev. A 83 (2011) 032303.
- [20] M. J. Biercuk, H. Uys, A. P. VanDevender, N. Shiga, W. M. Itano, J. J. Bollinger, Optimized dynamical decoupling in a model quantum memory, Nature 458 (2009) 996.
- [21] J. Du, X. Rong, N. Zhao, Y. Wang, J. Yang, R. B. Liu, Preserving electron spin coherence in solids by optimal dynamical decoupling, Nature 461 (2009) 1265.
- [22] G. A. Álvarez, A. Ajoy, X. Peng, D. Suter, Performance comparison of dynamical decoupling sequences for a qubit in a rapidly fluctuating spin bath, Phys. Rev. A 82 (2010) 042306.
- [23] E. R. Jenista, A. M. Stokes, R. T. Branca, W. S. Warren, Optimized, unequal pulse spacing in multiple echo sequences improves refocusing in magnetic resonance, J. Chem. Phys. 131 (2009) 204510.
- [24] A. M. Stokes, Y. Feng, T. Mitropoulos, and W. S. Warren, Enhanced refocusing of fat signals using optimized multipulse echo sequences, Magn Reson Med. 69 (2012) 1044.
- [25] R. Tycko, Broadband population inversion, Phys. Rev. Lett. 51 (1983) 775.
- [26] M. H. Levitt, Composite pulses, Prog. NMR Spect. 18 (1986) 61.

- [27] H. K. Cummins, J. A. Jones, Use of composite rotations to correct systematic errors in NMR quantum computation, *New J. Phys.* 2 (2000) 6.
- [28] H. K. Cummins, G. Llewellyn, J. A. Jones, Tackling systematic errors in quantum logic gates with composite rotations, *Phys. Rev. A* 67 (2003) 042308.
- [29] W. G. Alway, J. A. Jones, Arbitrary precision composite pulses for NMR quantum computing, *J. Magn. Res.* 189 (2007) 114.
- [30] S. Pasini, T. Fischer, P. Karbach, G. S. Uhrig, Optimization of short coherent control pulses, *Phys. Rev. A* 77 (2008) 032315.
- [31] S. Pasini, G. S. Uhrig, Generalization of short coherent control pulses extension to arbitrary rotations, *J. Phys. A: Math. Theo.* 41 (2008) 312005.
- [32] S. Pasini, P. Karbach, C. Raas, G. S. Uhrig, Optimized pulses for the perturbative decoupling of spin and decoherence bath, *Phys. Rev. A* 80 (2009) 022328.
- [33] B. Fauseweh, S. Pasini, G. S. Uhrig, Frequency-modulated pulses for quantum bits coupled to time-dependent baths, *Phys. Rev. A* 85 (2012) 022310.
- [34] K. Khodjasteh, L. Viola, Dynamically error-corrected gates for universal quantum computation, *Phys. Rev. Lett.* 102 (2009) 080501.
- [35] K. Khodjasteh, D. A. Lidar, L. Viola, Arbitrarily accurate dynamical control in open quantum systems, *Phys. Rev. Lett.* 104 (2010) 090501.
- [36] T. J. Green, J. Sastrawan, H. Uys, M. J. Biercuk, Arbitrary quantum control of qubits in the presence of universal noise, *New J. Phys.* 15 (2013) 095004.
- [37] W. S. Warren, Effects of arbitrary laser or NMR pulse shapes on population inversion and coherence, *J. Chem. Phys.* 81 (1984) 5437.
- [38] J. H. Gutow, M. McCoy, F. Spano, W. S. Warren, Crafted pulses for the uniform suppression of a region in a coherent spectrum, *Phys. Rev. Lett.* 55 (1985) 1090.
- [39] D. Horita, P. Hajduk, L. Lerner, Theoretical analysis of relaxation during shaped pulses. II. The effects of cross relaxation, *J. Mag. Res.* 103 (1993) 53.
- [40] J. Shen, L. Lerner, Selective radiofrequency pulses minimizing relaxation, *J. Mag. Res.* 112 (1995) 265.
- [41] T. E. Skinner, T. O. Reiss, B. Luy, N. Khaneja, S. J. Glaser, Application of optimal control theory to the design of broadband excitation pulses for high-resolution NMR, *J. Mag. Res.* 163 (2003) 8.
- [42] K. Kobzar, T. E. Skinner, N. Khaneja, S. J. Glaser, B. Luy, Exploring the limits of broadband excitation and inversion pulses, *J. Mag. Res.* 170 (2004) 236.
- [43] P. Sengupta, L. P. Pryadko, Scalable design of tailored soft pulses for coherent control, *Phys. Rev. Lett.* 95 (2005) 037202.
- [44] M. Möttönen, R. de Sousa, J. Zhang, K. B. Whaley, High-fidelity one-qubit operations under random telegraph noise, *Phys. Rev. A* 73 (2006) 022332.
- [45] L. P. Pryadko, G. Quiroz, Soft-pulse dynamical decoupling in a cavity, *Phys. Rev. A* 77 (2008) 012330.
- [46] L. P. Pryadko, P. Sengupta, Second-order shaped pulses for solid-state quantum computation, *Phys. Rev. A* 78 (2008) 032336.
- [47] A. M. Souza, G. A. Álvarez, D. Suter, Robust dynamical decoupling, *Phil. Trans. R. Soc. Lond. A* 370 (2012) 4748.
- [48] M. J. Biercuk, H. Bluhm, Phenomenological study of decoherence in solid-state spin qubits due to nuclear spin diffusion, *Phys. Rev. B* 83 (2011) 235316.
- [49] D. Stanek, C. Raas, G. S. Uhrig, Dynamics and decoherence in the central spin model in the low-field limit, *Phys. Rev. B* 88 (2013) 155305.
- [50] J. Hackmann, D. S. Smirnov, M. M. Glazov, F. B. Anders, Spin noise in a quantum dot ensemble: From a quantum mechanical to a semi-classical description, *arXiv:1403.3550*.
- [51] J. R. Klauder, P. W. Anderson, Spectral diffusion decay in spin resonance experiments, *Phys. Rev.* 125 (1962) 912.
- [52] G. de Lange, Z. H. Wang, D. Ristè, V. V. Dobrovitski, R. Hanson, Universal dynamical decoupling of a single solid-state spin from a spin bath, *Science* 30 (2010) 60.
- [53] A. Abragam, *The Principles of Nuclear Magnetism*, The International Series of Monographs on Physics, Clarendon Press, Oxford, 1978.
- [54] G. S. Uhrig, S. Pasini, Efficient coherent control by optimized sequences of pulses of finite duration, *New J. Phys.* 12 (2010) 045001.
- [55] S. Pasini, P. Karbach, G. S. Uhrig, High order coherent control sequences of finite-width pulses, *Europhys. Lett.* 96 (2011) 10003.
- [56] R. Bhatia, *Matrix Analysis*, Vol. 169 of Graduate Texts in Mathematics, Springer Verlag, New York, 1997.
- [57] S. Blanes, F. Casas, J. A. Oteo, J. Ros, The Magnus expansion and some of its applications, *Phys. Rep.* 470 (2009) 151.
- [58] C. Stihl, Optimierung von Pulsen zur Entkopplung eines Spins von klassischem Rauschen: Amplituden- und Frequenzmodulation gegen Dephasierung und Dekohärenz, Diploma Thesis, available at <http://t1.physik.uni-dortmund.de/uhrig/diploma.html>, TU Dortmund, 2012.
- [59] A. Alvermann, H. Fehske, High-order commutator-free exponential time-propagation of driven quantum systems, *J. Comput. Phys.* 230 (2011) 5930.
- [60] A. Alvermann, H. Fehske, P. B. Littlewood, Numerical time propagation of quantum systems in radiation fields, *New J. Phys.* 14 (2012) 105008.
- [61] Z.-Y. Wang, R.-B. Liu, No-go theorems and optimization of dynamical decoupling against noise with soft cutoff, *Phys. Rev. A* 87 (2013) 042319.
- [62] G. A. Álvarez, D. Suter, Measuring the spectrum of colored noise by dynamical decoupling, *Phys. Rev. Lett.* 107 (2011) 230501.
- [63] J. H. V. Vleck, The dipolar broadening of magnetic resonance lines in crystals, *Phys. Rev.* 74 (1948) 1168.
- [64] P. A. Beckmann, Spectral densities and nuclear spin relaxation in solids, *Phys. Rep.* 171 (1988) 85.